JOURNAL OF CATALYSIS 146, 144–154 (1994)

Effect of the K–Mo Interaction in K–MoO_3/γ-Al_2O_3 Catalysts on the Properties for Alcohol Synthesis from Syngas

Ming Jiang, Guo-Zhu Bian, and Yi-Lu Fu[1]

Department of Modern Chemistry, University of Science and Technology of China, Hefei, Anhui 230026, People's Republic of China

Received March 8, 1993; revised July 8, 1993

A series of K–MoO_3/γ-Al_2O_3 catalysts was prepared by varying the K/Mo atomic ratios between 0 and 1.5, maintaining molybdenum content as constant. The structures of the samples were characterized by several techniques (LRS, XRD, XPS, ESR, TPR, O_2, CO and H_2 chemisorption, and TPD) and accounted for the catalytic properties for alcohol synthesis from synthesis gas. It is revealed that for the potassium-promoted samples an interaction between the potassium promoter and the supported molybdenum component occurs. The amount of the species resulting from this interaction gets saturated at a K/Mo ratio of 0.8. On the oxidic samples, K–Mo interaction species which may contain potassium cations and an $Mo_7O_{24}^{6-}$ unit are formed. This retards, to some extent, the sulfidation and reduction of Mo(VI) to Mo(IV). The sulfidation of the interaction species leads to the aggregation of MoS_2 and the formation of surface "K–Mo–S" species. At K/Mo ratios above 0.8, KCl crystallites form; some amount of KCl, which is not aggregated, covers the exposed molybdenum surface, and decreases the amount of "K–Mo–S" species and Mo(CUS) sites. The activity toward alcohol formation over the sulfided samples is in parallel with the extent of the K–Mo interaction, with the maximum achieved at K/Mo ratio of 0.8, while alcohol selectivity monotonically increases with K/Mo ratio. It is tentatively proposed that the surface "K–Mo–S" species and Mo(CUS) sites are responsible for the alcohol and hydrocarbon formations, respectively. The large increase in alcohol selectivity at K/Mo ratios above 0.8 could be attributed to the effect of the unaggregated KCl which preferentially covers the Mo(CUS) sites. The high $C_{2+}OH/C_1OH$ ratio in the alcohol product distribution is probably due to the substantial amount of the SH species present on the surface of the sulfided samples during reaction.

INTRODUCTION

Molybdenum-based catalysts with modification of alkali promoters have been claimed to have excellent properties for alcohol synthesis from synthesis gas and to be sulfur tolerant. Interests in the catalyst systems have been heightened by the worldwide challenge for upgrading low-grade energy sources such as coal. Dow Chemical and Union Carbide Scientists (1–3) have claimed in a number of patents about the molybdenum sulfide catalysts promoted by cobalt or alkali components, over which alcohol products of C_1–C_5 were obtained. The effect of pressure on alcohol synthesis over the K_2CO_3-promoted MoS_2 catalysts was reported by Xie *et al.* (4). The work of Klier *et al.* (5) on $CsOH/MoS_2$ catalysts indicates that alkali promoter loading is an important factor which affects the performance of the catalysts for alcohol synthesis, the optimum for alcohol formation being achieved at a certain promoter loading. Similar results were obtained over K_2CO_3/MoS_2, reduced K–Mo/SiO_2, sulfided K–Mo/SiO_2 and K–Mo/ZrO_2 catalysts (6–8). A method was developed by Woo *et al.* (9) to prepare K_2CO_3/Mo_2C catalysts by impregnation of Mo_2C with a K_2CO_3 solution. The molybdenum carbide was obtained from calcination of MoO_3 powder in an atmosphere of CH_4/H_2 at 400–700°C. Tatsumi *et al.* (10) reported the effect of potassium promoters added in different forms on alcohol synthesis over the reduced Mo/SiO_2 catalysts and found that KCl is the most favorable promoter for alcohol synthesis in their case. The role of alkali promoter played in molybdenum catalysts is still a matter of intense debate. Klier *et al.* (5) proposed that the catalysts for alcohol synthesis should be bifunctional and composed of an alkali promoter, which enhances activation of CO, and molybdenum sulfide, which activates H_2 adsorption. From temperature-programmed desorption of CO and H_2 adsorbed on K_2CO_3/MoS_2 catalysts (6), a similar conclusion was drawn that the addition of the potassium promoter to the catalysts with an appropriate content causes increase in CO uptake and decrease in H_2 uptake, paralleled by an increase in selectivity toward alcohol formation. A new surface phase was proposed by Xie *et al.* (6) based upon the catalyst characterization by X-ray diffraction, X-ray photoelectron spectroscopy, and electron diffraction, and suggested to be active for alcohol synthesis. For supported catalysts, the molybdenum component interacts with the support and could be well dispersed. The role that the promoter played in the catalysts could be different from that in unsupported catalysts. The results from X-ray photoelec-

[1] To whom correspondence should be addressed.

0021-9517/94 $6.00

tron spectra show that the reducibility of Mo(VI) in Mo/γ-Al_2O_3 catalysts is, to some extent, inhibited by the potassium promoter (11, 12). The inhibition effect of the potassium promoter on the dispersion of molybdenum as well as on the reduction of Mo(VI) on the reduced K–Mo/SiO_2 catalysts was also observed and accounted for performance of the catalysts for alcohol synthesis (13).

The previous works on the molybdenum catalysts used for alcohol synthesis, most of them dealt with unsupported catalysts with alkali modifiers, while few dealt with supported ones. There are many issues which are still not understood about the effect of alkali promoters on structures and catalytic properties of sulfided molybdenum catalysts. The aim of the present work is to explore the role of the potassium promoter in Mo/γ-Al_2O_3 catalysts. A series of Mo/γ-Al_2O_3 catalysts with different potassium loading was prepared and investigated for activity and selectivity toward alcohol formation. The interaction between the potassium promoter and the molybdenum component and its effect on the reducibility, sulfidability, and dispersion of the molybdenum species on the samples were elucidated based upon characterization by laser raman spectroscopy, X-ray diffraction, X-ray photoelectron spectroscopy, electron spin resonance, temperature-programmed reduction, probe molecule chemisorption, and temperature-programmed desorption. The catalyst structures and catalytic properties for alcohol synthesis were correlated.

EXPERIMENTAL

1. Sample Preparations

The support γ-Al_2O_3 was obtained from $Al(OH)_3$ (Institute of Tianjing Chemical Engineering) by calcination at 750°C for 16 h. The N_2 BET surface area of this support material was 270 m^2/g.

The oxidic samples were prepared by sequential impregnation of the support with the aqueous KCl solutions, followed by drying at 120°C for 12 h and calcination at 300°C for 1 h, and then impregnation with $(NH_4)_6Mo_7O_{24} \cdot 4H_2O$, followed by drying and calcination at 500°C for 24 h. The unpromoted sample was prepared just following the latter step.

The mixture of CS_2/H_2 (ca. 8.7%), used as sulfiding gas, was obtained by passing H_2 through 0°C CS_2 liquid. The sulfided samples were obtained by sulfiding the oxidic samples in a flow (30 ml/min) of CS_2/H_2 at 400°C for 6 h.

The molybdenum content in the samples, expressed as wt% MoO_3 of γ-Al_2O_3, was 24%, and potassium, as K/Mo atomic ratio, varied from 0 to 1.5.

2. Characterization Methods

(*1*) *Laser Raman spectroscopy* (*LRS*). Spectra were run on a Spex-1403 spectrometer using the 488.0-nm line from a Spectra-Physics-2020 argon laser. The laser beam intensity engaged was 150 mW for the oxidic samples and 200 mW for the sulfided samples. The spectrum slit width was 3.5 cm^{-1} and the spectrometer resolution was ± 2 cm^{-1}. The samples were pressed into pellets for analyses.

(*2*) *X-ray diffraction* (*XRD*). XRD patterns were obtained with a D/MAX-γA rotatory target diffractometer using Cu $K\alpha$ radiation. The sample was ground into fine powders and packed in a sample holder for measurements.

(*3*) *X-ray photoelectron spectroscopy* (*XPS*). Spectra were recorded on an ESCA LAB MK-II spectrometer using an Al $K\alpha$ X-ray source (1486.6 eV). The pressure in the sample chamber was around 4×10^{-7} Pa. The Al_{2p} peak (74.5 eV) from the samples was used as internal standard for binding energy calibration. The atomic ratios of the surface species on the sulfided samples were calculated from peak areas according to Wagner's sensitivity factors (14).

(*4*) *Electron spin resonance* (*ESR*). Spectra were taken in the X-band on an ER 200R-SRC spectrometer operating at 9.76 GHz at room temperature.

(*5*) *Temperature-programmed reduction* (*TPR*). TPR of the oxidic samples was carried out with a mixture of H_2/N_2 (1 : 9) at atmosphere pressure in a conventional TPR setup. The gas mixture (30 ml/min), which was purified by passing through the 105 deoxy agent (produced by Hepin Street Chemical Plant, Beijing) and zeolite 5A, was passed over an oxidic sample placed in a steel tube reactor. The temperature of the sample was increased linearly at a rate of 10°C/min. The hydrogen concentration was continuously monitored by a thermal conductivity detector attached to a gas chromatograph and evaluated by a Shimadzu C-R3A electronic integrator.

(*6*) *O_2, CO, and H_2 chemisorption and H_2 temperature-programmed desorption* (*TPD*). The chemisorption of O_2, CO, and H_2 on the sulfided samples was performed on a chromatographic system by using a pulse technique. The sample (0.2 g) was first treated in a flow (20 ml/min) of H_2 at 400°C for 1 h and then in a flow of argon (nominal purity 99.99%) at 450°C for 3 h. The sample was finally cooled to 300°C for H_2 adsorption measurement or cooled to −83.6°C for O_2 or CO adsorption measurement by inserting the U-type reactor into a mixed paste of liquid nitrogen and ethylacetate after the sample was naturally cooled to ambient temperature. Pulses of the adsorption gas were directed into the argon carrier gas which passed through the sample bed and then into a thermal conductivity detector in a gas chromatograph for detection of the unadsorbed H_2, O_2, and CO. The adsorption was taken as saturated after typically 3–7 pulses when the areas of the successive outlet pulses were equal. The sample saturated with adsorbed H_2 at 300°C was cooled to 90°C

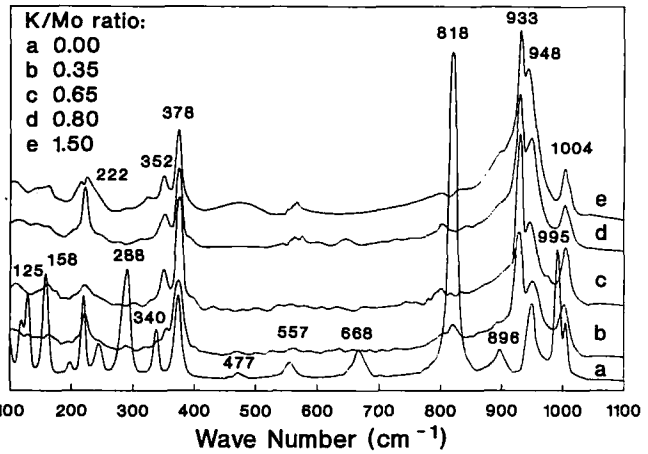

FIG. 1. Raman spectra of the oxidic K–MoO_3/γ-Al_2O_3 samples with different K contents.

in a flow of H_2 (20 ml/min) and stood at that temperature in a flow of argon until the base line of the gas chromatograph remained constant and then subjected to temperature-programmed desorption of H_2. The desorption was displayed on a Shimadzu C-R3A integrator.

3. *Catalytic Reaction Measurements*

The catalytic conversion of CO to alcohols over the sulfided samples was measured with a fixed bed flow reactor equipped with a on-line gas chromatograph. The synthesis gas was composed of CO 33%, H_2 55%, and N_2 12%. Each experiment was performed using 0.5 ml of sample. The effluent gas from the reactor was directed into a sample valve on a gas chromatograph and analyzed by a flame ionization detector with a Porapak Q column for separating the hydrocarbon and alcohol products and a thermal conductivity detector with a TDX-01 column for CO, CO_2, H_2, and N_2. under the present experimental conditions, only a trace amount of CO_2 could be detected by the thermal conductivity detector, thus the conversion of CO mentioned below would be preferred to that with CO_2 free.

RESULTS

1. *LRS*

Raman spectra of the oxidic samples are shown in Fig. 1. Bulk MoO_3 was obviously detected in the Raman spectra of the unpromoted sample. In Fig. 1a, the frequencies of γ-Al_2O_3-supported MoO_3 (995, 818, 668, 378, 340, 288, 222, 198, 158, 125, and 115 cm^{-1}) are almost identical to those of bulk MoO_3 (19), with only minor differences observed in the low-frequency region. The bands at 1004 and 378 cm^{-1}, the latter coinciding with the band of MoO_3 occurring at the same position, are characteristic of $Al_2(MoO_4)_3$, a species resulting from a strong interaction of the molybdenum with the support. Fully oxidized molybdenum can be tetrahedrally or octahedrally coordinated and forms surface molybdenum species on γ-Al_2O_3 at a low molybdenum loading. In an aqueous solution, molybdenum forms isolated Mo(Td) (MoO_4^{2-}) above pH 7–8 which has Raman bands of 896, 843, and 317 cm^{-1}, and octahedrally coordinated molybdenum (Mo(Oh)) clusters at a lower pH, such as $Mo_7O_{24}^{6-}$ with the Raman bands at 941, 896, 360, and 219 cm^{-1} (15, 16, 20). The most intense band is commonly due to the symmetric stretching mode. The vibration modes, especially the stretching mode, of the Mo(Td) and Mo(Oh) in the aqueous solution, by comparison, can be used to assign the vibrations of the supported surface molybdenum species. Thus, the additional bands detected in the spectra of Fig. 1a can be assigned to the species of Mo(Td) (896 cm^{-1}) and polymolybdate of Mo(Oh) (948 cm^{-1}). Some authors suggested that the molybdenum oxo species should be dispersed on γ-Al_2O_3 in a monolayer at a molybdenum loading lower than that for monolayer coverage (17). Our Raman spectrum results presented here clearly show the formation of crystalline MoO_3 on the support although the molybdenum loading is only about two-thirds of that for monolayer coverage, which is in accord with the previous results obtained in our laboratory (18). The discrepancy between other authors' results and ours could result from the differences in the γ-Al_2O_3 used and the conditions employed for catalyst preparation.

The formation of the Mo(Td) species, especially in the supported MoO_3, is greatly suppressed with addition of the potassium promoter to the samples (Figs. 1b–1e). A very weak band at 818 cm^{-1}, the most intense band for MoO_3, can still be detected in the Raman spectra of the sample with a K/Mo ratio of 0.35; it disappears with a higher K/Mo ratio. The band around 896 cm^{-1} which is related to the surface Mo(Td) species is hardly detected in the spectra of the potassium-promoted samples. The band intensities of the surface Mo(Oh) species and $Al_2(MoO_4)_3$ do not significantly change as potassium loading increases. The new bands, compared to the unpromoted sample, appear at 933, 352, and 222 cm^{-1} for the potassium-promoted samples, and as potassium loading increases their strengths increase and pass through a maximum at a K/Mo ratio of 0.65–0.8 and decrease at a higher K/Mo ratio. Raman spectroscopy can be used to detect both supported crystalline compounds such as the supported MoO_3 and the surface species of the supported molybdenum oxides such as the surface Mo(Td) and Mo(Oh) species, as discussed above. In an aqueous solution, $Mo_7O_{24}^{6-}$ ion possesses four main Raman bands. However, more bands are commonly observed in the crystal-

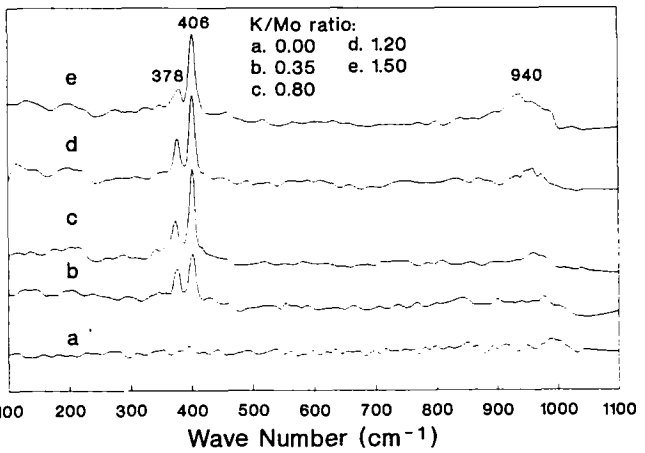

FIG. 2. Raman spectra of the sulfided K–MoO_3/γ-Al_2O_3 samples with different K contents.

line compounds containing an $Mo_7O_{24}^{6-}$ unit because of the geometrical distortion due to crystalline formation. An appropriate and direct way to identify supported crystalline compounds is to compare their Raman spectra with those of the analogous unsupported compounds. The features of the new bands occurring for the potassium-promoted samples are comparable to those for the unsupported $(NH_4)_6Mo_7O_{24} \cdot 4H_2O$ compound which has the main raman frequencies at 933, 375, 363, and 224 cm^{-1} (15). Obviously, a polymolybdate species containing an $Mo_7O_{24}^{6-}$ unit forms on the surface of γ-Al_2O_3. The intensity of the band at 378 cm^{-1} varies with the K/Mo ratio with the same trend as that at 933 cm^{-1} from the polymolybdate species, while the intensity of the band at 1004 cm^{-1} from $Al_2(MoO_4)_3$ is almost unchanged as the K/Mo ratio increases. So the band at 378 cm^{-1} should be from the overlap of the bands occurred at same position from both $Al_2(MoO_4)_3$ and the polymolybdate species.

Raman spectra of the sulfided samples are shown in Fig. 2. For the unpromoted sample (Fig. 2a), there is hardly any observable band which could be assigned to the sulfided molybdenum species, indicating that the molybdenum species are well dispersed on the support after sulfidation under our conditions. Upon addition of potassium promoter to the samples (Figs. 2b–2e), the bands at 378 and 406 cm^{-1}, characteristic of MoS_2, are significantly pronounced and their intensities increase as potassium loading increases and level off at a K/Mo ratio of 0.65–0.8. The further increase in the potassium loading does not increase, but slightly decreases, the intensities of the bands for MoS_2. Moreover, a broad band at 880–990 cm^{-1} becomes observable at K/Mo ratio of 0.65 and is more pronounced at a higher K/Mo ratio. The broad feature could be ascribed to the surface oxysulfide species, as suggested by Schrader and Cheng (19), and is associated with the extent of sulfidation of the molybdenum components.

2. XRD

XRD patterns of the oxidic and sulfided samples are shown in Fig. 3. The XRD technique is much less sensitive than Raman spectroscopy. In Fig. 3a, the XRD pattern of the unpromoted oxidic sample is almost identical to that of the amorphous support. The surface oxidic Mo(Td) and Mo(Oh) species and supported MoO_3, as clearly detected by LRS, are not observed, indicating that the surface molybdenum species are amorphous and the MoO_3 crystalline domains are too small to give rise to a XRD pattern. A new set of diffractions for the potassium-promoted oxidic samples, however, clearly appear at *d*-values of 0.397, 0.285, and 0.276 nm. The diffraction intensities increase as potassium loading increases and reach their maxima at a K/Mo ratio of 0.8 and decrease at a higher potassium loading. Compared with LRS results for the potassium-promoted samples, the new diffractions could be assigned to the interaction species which is composed of the potassium promoter and the molybdenum component and might contain the $Mo_7O_{24}^{6-}$ unit. The variation of the intensities with potassium loading from the XRD patterns closely matches that from LRS. At a K/Mo ratio above 0.8, the XRD patterns of the oxidic samples clearly show the presence of a crystalline KCl compound with diffractions at *d*-values of 0.314, 0.222, and 0.181 nm, the intensities increasing as the K/Mo ratio increases. After sulfidation, the diffractions assigned to the interaction species of the potassium promoter and the molybdenum component completely disappear, while those assigned to the crystalline KCl compound almost keep the same intensities as those prior to sulfidation (Fig. 3b). A very weak broad feature appears at a *d*-value of around

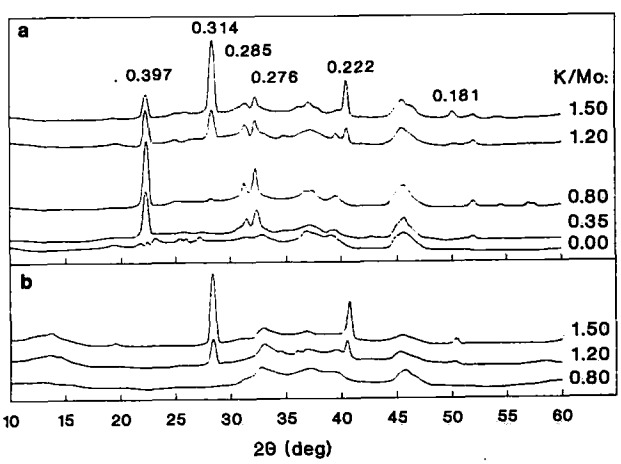

FIG. 3. XRD patterns of the oxidic (a) and sulfided (b) K–MoO_3/γ-Al_2O_3 samples with different K contents.

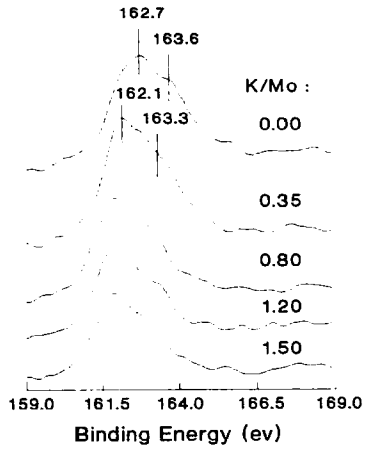

FIG. 4. S_{2p} XPS spectra of the sulfided K–MoO_3/γ-Al_2O_3 samples.

0.69 nm, indicating the evolution of the poorly crystallized MoS_2.

3. XPS

The binding energy of the $Mo_{3d_{5/2}}$ peak of all the oxidic samples is 233.1 eV, which is close to that of MoO_3 (14), indicating the presence of Mo(VI) on the oxidic samples. The binding energies of $Mo_{3d_{5/2}}$ for all the sulfided samples are around 229.2 eV, which is the same as that for MoS_2 (14). The S_{2p} spectra for the sulfided samples shown in Fig. 4 are rather complicated. The major component in the spectra is S^{2-} with a binding energy at ca. 162.3 eV, which is close to that for MoS_2 (14). A shoulder component is also observed in the spectra at a binding energy of around 163.3 eV. The value is between the binding energies of elemental sulfur (ca. 164 eV) and of the sulfur in MoS_2 (162.1 eV). Within this range is binding energy reported for di- and polysulfide species which contain S_2^{2-} ligands with a binding energy between 162.3–164.4 eV (21, 22). In addition, two very weak signals are observable in the spectra at 165 and 168 eV, indicating that very small amount of high-valence sulphus species, S(4+) and S(6+), appears on the sample surfaces. As potassium is added, there are decreases in the areas of the peaks due to S^{2-} and S_2^{2-} and concurrent shifts of the binding energies to lower positions. The O_{1s}, K_{2p}, and Cl_{2p} spectra were also recorded for all the oxidic and sulfided samples. Their binding energies are close to those of MoO_3 (O_{1s}, 531.5 eV), KCl (K_{2p}, 292.7 eV), and KCl (Cl_{2p}, 198.9 eV) (14), respectively.

Figure 5 shows the dependence of the atomic ratios of the species on the sulfided samples upon the potassium loading, which were calculated from the areas of the XPS peaks of Mo_{3d}, K_{2p}, Cl_{2p}, and the deconvoluted S^{2-} and S_2^{2-}. Because the detection depth of the XPS technique is limited below ca. 2 nm from the surface, the atomic ratios determined by XPS should represent the information of the surface layer, or more exactly, a few surface layers of the samples, and therefore can be regarded as the surface atomic ratios. The surface S^{2-}/Mo atomic ratio for the unpromoted sample is slightly higher than the stoichiometric value, 2, in MoS_2. This value is similar to that obtained by XPS determinations for Mo/γ-Al_2O_3 sulfided with CS_2/H_2 at 400°C by Okamoto *et al.* (23) and that for the sulfided molybdenum thin film by Spevack and McIntyre (24). The surface atomic ratios of S^{2-}/Mo and S_2^{2-}/Mo decrease monotonically with increasing potassium loading, indicating an inhibition effect of the potassium promoter on sulfidation of the oxidic molybdenum species. The surface K/Mo ratio of the samples increases as potassium loading increases and levels off at a K/Mo ratio of 0.8. It is interesting to note, however, that the surface K/Mo ratios are always larger than the K/Mo ratios used in sample preparations, that is, the bulk K/Mo ratios. This result allows us to conclude that an enrichment of the potassium cations onto the sample surface occurs especially at a low potassium loading. At a K/Mo ratio above 0.8, the surface K/Mo ratio does not significantly increase, indicating that the enrichment gets saturated. The XPS signals of the Cl_{2p} for the samples are rather weak and the errors in the absolute surface Cl^- concentrations based upon the calculations of Cl_{2p} intensities could not be ignored. But the variation of the relative surface Cl^- concentration versus potassium loading should be reliable for comparison. As shown in Fig. 5, the surface Cl/K ratios are much lower than the Cl/K ratio in the added KCl promoter at a K/Mo ratio below 0.8. Even for the sample with a K/Mo ratio of 0.8, the calcu-

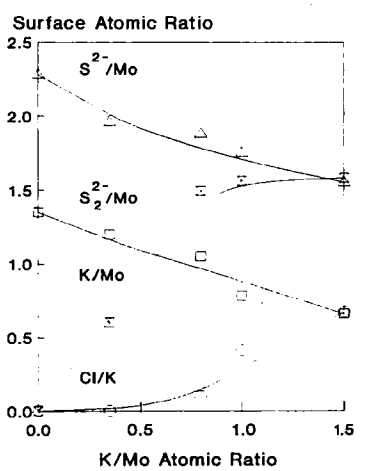

FIG. 5. Surface atomic ratios of sulfided K–MoO_3/γ-Al_2O_3 samples from XPS determinations versus potassium loadings.

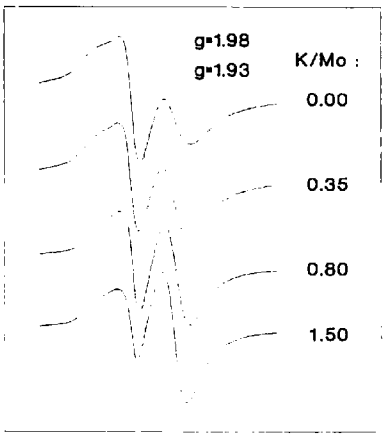

FIG. 6. ESR spectra of the sulfided K–MoO_3/γ-Al_2O_3 samples with different K contents.

lated surface Cl/K ratio is still very low, being only about 0.1. At a higher potassium loading, the surface Cl/K ratio increases, which is probably due to formation of KCl.

4. ESR

The hexavalent molybdenum species is not paramagnetic and gives no ESR signal. Both pentavalent and tetravalent molybdenum species are paramagnetic, but the ESR signal due to Mo(IV) is likely to be very broad and not detectable at room temperature, while the resonance absorption due to Mo(V), in a suitable environment, is readily observable even at room temperature. When supported on γ-Al_2O_3, due to the interaction of the molybdenum component with the support, hexavalent Mo(VI) is converted, to some extent, to the pentavalent state during calcination in catalyst preparation, and therefore an ESR signal is observed at a g-value of ca. 1.93, which is due to Mo(V) in an environment of axial symmetry. The Mo(V) signal, with addition of potassium promoter to the oxidic samples, becomes less intense (not shown in figure). The sulfided samples give much more intense Mo(V) signals than the oxidic samples. Figure 6 shows the ESR spectra of the sulfided samples. The signal intensities in the spectra for all the samples in this figure are depicted based upon the same atomic concentration of molybdenum and can directly be used for comparing the concentrations of the paramagnetic species. In contrast to the oxidic samples, the intensities of Mo(V) ESR signal for the sulfided samples increase with potassium loading. In addition, a new signal around a g-value of ca. 1.98 is intense for all the sulfided samples. This signal, in view of its absence in the case of Mo/Al_2O_3 sulfided with H_2S/H_2 (25), instead of the CS_2/H_2 mixture, could be attributed to the carbon ions resulting from the sample sulfidation in CS_2/H_2. As potassium loading increases, the intensity of the carbon ion signal varies inversely, in contrast to that of Mo(V).

5. TPR

TPR experiments were performed for all the oxidic samples. Figure 7 shows the H_2 consumption as a function of temperature. Reduction of the samples started at 100°C and was completed at 800°C. The TPR of pure MoO_3 was also carried out as a reference and the result indicates that the reduction peak which corresponds to the transformation of Mo(VI) to Mo(IV) is observed at about 730°C, similar to the TPR result of MoO_3 obtained by Ismail *et al.* (26). The reduction of Mo(VI) to Mo(IV) for the γ-Al_2O_3 supported molybdenum oxide as shown in Fig. 7 shifts to a much lower temperature, suggesting a support effect. For the unpromoted sample, the reduction peak is centered at about 480°C. In addition to this, some weak features occur at higher temperature positions and become more pronounced at a low potassium loading with a K/Mo ratio of 0.35, indicating that more than one kind of oxidic Mo(VI) species exist on the support, consistent with the LRS results, as discussed above. Upon a further increase in the potassium loading in the sample, the temperature of the peak due to the reduction of Mo(VI) to Mo(IV) gradually shifts to 555°C and remains unchanged at K/Mo ratios above 0.8.

6. O_2, CO, and H_2 chemisorption and H_2 TPD

The relative chemisorption data of O_2 and CO at −83.6°C and of H_2 at 300°C for the sulfided samples are summarized in Fig. 8. The uptake by the pure γ-Al_2O_3 under identical experimental conditions was taken into account to make corrections for the uptakes of all the sulfided samples.

The choice of the temperature at which O_2 chemisorption could give useful information on the surface structures of the sulfided molybdenum catalysts is a very important factor, as claimed by many authors (27–29). It

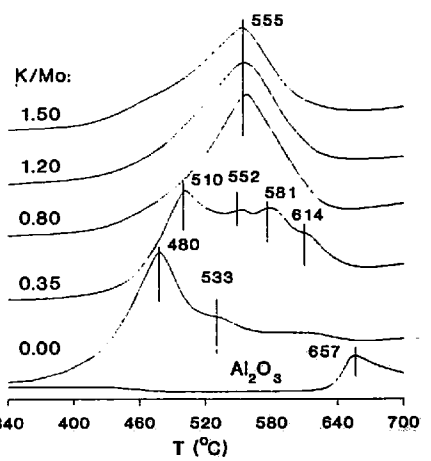

FIG. 7. TPR patterns of the oxidic K–MoO_3/γ-Al_2O_3 samples with different K contents.

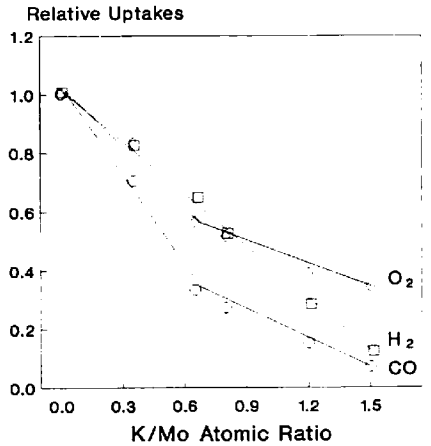

FIG. 8. Relative chemisorption uptakes of O_2, CO, and H_2 over the sulfided K–MoO_3/γ-Al_2O_3 samples.

was found that the temperature of around −78°C was the most suitable for oxygen chemisorption and that at room temperature the information from oxygen chemisorption could be obscured, probably by the chemical interaction of oxygen with the sulfided molybdenum surface. Therefore, a low temperature of −83.6°C was chosen in the present work for oxygen chemisorption. The pulse experiment of CO adsorption at room temperature were also performed for all the sulfided samples, but only very low uptakes were obtained, hence the method is not suitable for characterization purposes. At a low temperature of −83.6°C, the uptakes of CO adsorption are, however, of the same order of magnitude as those of O_2 on the identical samples. The pulse adsorption of H_2 on the sulfided samples could only be observed at the temperature above 100°C. A higher temperature, commonly 300°C, is necessary to obtain appreciable chemisorption (29, 30). For comparative purpose, the O_2, CO, and H_2 chemisorption data compared in Fig. 8 are on a relative instead of a quantitative basis, which should be more suitable for understanding the effects of the potassium promoter. It is interesting to note that the O_2, CO, and H_2 adsorption capacities of the sulfided samples are suppressed by the addition of the potassium promoter. For the sample with a K/Mo ratio of 1.5, the uptakes of O_2, CO, and H_2 are only about one-third, one-tenth, and one-tenth of those for the unpromoted sample, respectively. However, the variations of the O_2, CO, and H_2 adsorption capacity with potassium loading are not the same. A slope change can apparently be observed for O_2 and CO adsorption at a K/Mo ratio of 0.65–0.8, above which the uptakes decline less rapidly as the K/Mo ratio increases. For H_2 adsorption, however, the uptake decreases almost linearly, with the K/Mo ratio varying between 0–1.5. This difference, as discussed below, could be attributed to the H_2 adsorption mechanism, which is different from those for both O_2 and CO.

The sulfided samples saturated with adsorbed hydrogen were subjected to TPD experimetns. The TPD patterns are shown in Fig. 9. At temperatures between 300–500°C one desorption peak is observed, consistent with the previous TPD results obtained in our laboratory (30). A high-temperature desorption peak (>450°C), which was absent in the case of H_2 TPD of the unsupported K_2CO_3/MoS_2 catalysts (6), is significantly intense for all the sulfided samples, and the peak temperature is typically 700°C or higher. The areas of both desorption peaks decrease as potassium loading increases. This trend is similar to that of the H_2 adsorption uptake versus K/Mo ratio.

7. *Catalytic Measurements*

All the sulfided samples were tested for alcohol synthesis. Long periods (typically over 100 h) were necessary to achieve a steady state in the reactions. Initial activity toward hydrocarbon formation was considerably higher than at steady state, while the activity toward alcohol formation increased gradually with the reaction time, even after 100 h on stream. But the variations of the activities for producing both hydrocarbons and alcohols with reaction time become less significant after reaction for about 15 h. For comparison purposes, the reaction results in Fig. 10 are presented for all the samples tested at 280°C, 4.0 MPa, and 4500 h^{-1} for 15 h. On the unpromoted sample, the conversion of CO toward alcohols is very low, and the predominant products are hydrocarbons. On the potassium promoted samples the hydrocarbon products are suppressed to some extent. A maximum of CO conversion to alcohols is developed on the sample with a K/Mo ratio of 0.8. With increasing potassium loading an increase in alcohol selectivity is observed, paralleled by decreases in hydrocarbon activity and selectivity. In addition, the

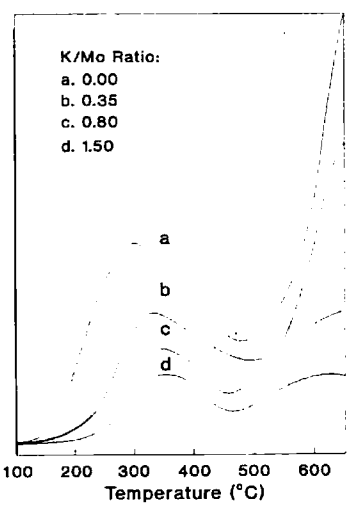

FIG. 9. H_2 TPD patterns of the sulfided K–MoO_3/γ-Al_2O_3 samples with different K contents.

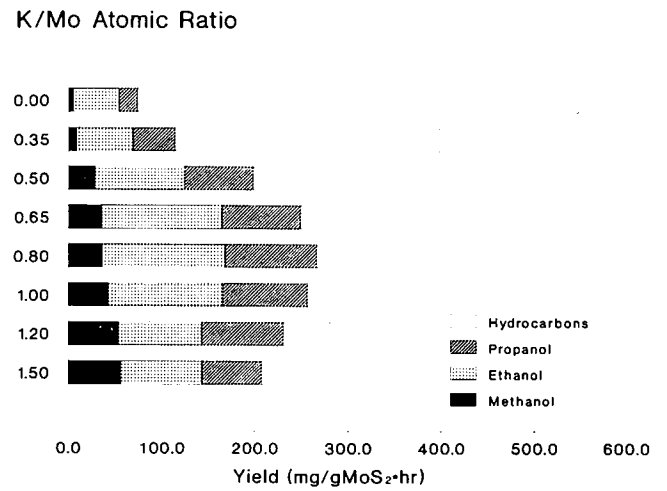

FIG. 10. Effect of the K loadings on the activity and selectivity toward alcohol formation from syngas. Reaction conditions: 280°C, 4.0 MPa, 4500 h^{-1}, and H_2/CO = 1.8.

alcohol products with high carbon number, $C_{2+}OH$, other than methanol, are predominant in the product distribution. But the methanol product increases as the K/Mo ratio increases.

DISCUSSION

1. K–Mo Interaction

The new species resulting from the interaction of the potassium promoter with molybdenum component supported on γ-Al_2O_3, denoted here as the K–Mo interaction species, existed on the potassium promoted oxidic samples as revealed by XRD patterns. The species should be identical to the species which contains potassium cations and $Mo_7O_{24}^{6-}$ units as evidenced by LRS characterization. In view of XRD technique much less sensitive than LRS, a conclusion can be drawn that on the potassium promoted samples the K–Mo interaction species is predominant, and the amount of the other species such as surface Mo(Td) and Mo(Oh), and $Al_2(MoO_4)_3$, though detected by LRS, is too low to give rise to the respective XRD patterns. It is evident that potassium loading is an important variable which affects the formation of the K–Mo interaction species. XRD results clearly demonstrate that the stoichiometric amount for potassium to form the interaction species is at a K/Mo ratio of 0.8. At lower K/Mo ratios, the potassium promoter almost completely interacts with the supported molybdenum component and gives rise to the increase in the intensities of the diffractions and Raman bands which are responsible for the interaction species as potassium loading increases. Conversely, potassium added in excess of that required for the formation of the interaction species forms a KCl compound which is unfavorable for the formation of the K–Mo interaction species, as indicated by the decrease in its XRD intensities. Upon sulfiding, the disappearance of the diffractions and Raman bands responsible for the K–Mo interaction species indicates that the Mo(VI) in this species can be converted to Mo(IV). But in contrast to the unpromoted sample, the Mo(IV) component on the potassium-promoted samples is harder to disperse on the support during sulfidation and therefore gives rise to the obvious appearance of MoS_2 crystallites, as revealed by LRS detection. The variation of the MoS_2 crystallite size as a function of potassium loading is similar to that of the crystallite size of the K–MO interaction species with the K/Mo ratio, namely, both become saturated at a K/Mo ratio of 0.8.

The fact that the K–Mo interaction is saturated at a K/Mo ratio of 0.8 is also evidenced by the phenomenon of potassium cation enrichment on the surface of the sulfided samples, as discussed above for XPS results. In view of the fact that MoS_2 crystallites appear upon sample sulfiding, it could be suggested that the potassium cations should be enriched on the Mo–S surfaces to form a surface species which we call the surface "K–Mo–S" species. The very low surface Cl/K atomic ratio at a low potassium loading is due to the Cl^- anion loss during sample preparation and because of the K^+ cations strongly interacting with the molybdenum sulfide species for the reduced KCl–MoO_3/SiO_2 catalysts, Tatsumi *et al.* (31) suggested that the Cl^- anion loss occurs in the reduction step. Similar anion loss is also observed in the preparation of K_2CO_3–Co–Mo/Al_2O_3 catalysts (32). Due to the strong interaction of the potassium cations with the molybdenum component, the CO_3^{2-} anions were significantly lost so that the C_{1s} signal from CO_3^{2-} on the samples almost escaped the detection of XPS technique. When the K–Mo interaction becomes saturated at a K/Mo ratio above 0.8, Cl^- anions combine with the surplus K^+ cations which do not interact with the sulfided molybdenum species, and even form KCl crystallites. The similar intense diffractions of the KCl crystallites for the oxidic and respective sulfided samples suggest that the sulfidation step does not substantially affect the KCl crystallites. The significant increase in the surface Cl/K atomic ratio at a higher potassium loading, however, allows us to postulate that a part of the formed KCl molecules aggregates into crystallites, but the other part exists randomly on the sample surface.

2. Effect of K–Mo Interaction on the Properties of Reduction and Sulfidation

Because of the interaction of Mo(VI) with γ-Al_2O_3, the supported Mo(VI) oxo species can lose their outer coordinated oxygen atoms and be converted, to some extent, to the Mo(V) species during calcination for oxidic sample preparation. Similar transformation of Mo(VI) to Mo(V)

also occurs in the evacuation step for treatment of MoO_3/TiO_2 and MoO_3/SiO_2 catalysts (33). The K–Mo interaction weakens the interaction of the Mo(VI) component with the support and promotes aggregation of Mo(VI) to prevent the transformation of Mo(VI) to Mo(V), as revealed by the decrease in the Mo(V) ESR intensities of the potassium-promoted oxidic samples. The inhibition effect of the potassium promoter on the reduction of Mo(VI) to a lower valence state is also revealed by TPR of the oxidic samples. The fact that the temperature (ca. 480°C) of the reduction peak which is responsible for the transformation of Mo(VI) to Mo(IV) is much lower for the unpromoted sample than that for MoO_3 reference compound suggests an interaction of Mo(VI) with the support. Upon addition of the potasium promoter to the samples, the interaction is weakened by the K–Mo interaction. Compared with the unpromoted sample, the reduction of Mo(VI) to Mo(IV) for the potassium-promoted samples becomes slightly difficult and shifts to a higher temperature. When the K–Mo interaction becomes saturated at a K/Mo ratio above 0.8, the reduction temperature keeps constant at ca. 555°C, whereas the reduction peak area decreases with a further increase in the potassium loading, demonstrating a further resistance to the reduction of Mo(VI) to Mo(IV). An analogous conclusion concerning XPS characterization for $K–Mo/Al_2O_3$ catalysts has been drawn by DeCanio *et al.* (11) that the extent of reduction is inversely proportional to the potassium loading on catalysts.

The resistance to the transformation of Mo(VI) to Mo(IV) resulting from the K–Mo interaction is also observed in the sulfidation of the potassium-promoted samples. According to the XPS determinations, the main sulfur species existing on the surfaces of the sulfided samples are S^{2-} and S_2^{2-}, and only a small amount of S(4+) and S(6+) is observed at binding energies of ca. 165 and 168 eV, respectively. On the point of sulfidation, the S^{2-}/Mo atomic ratio actually more properly reflects the extent of sulfidation of the supported oxidic molybdenum species. The Mo(VI), if sulfided in stoichiometry, would completely convert to Mo(IV), giving rise to an S^{2-}/Mo atomic ratio of 2, as that in MoS_2. Meanwhile, the actual S^{2-}/Mo ratios of all the potassium-promoted samples, especially the samples with high potassium loading, are significantly lower than this value, indicating that the potassium promoter inhibits the transformation of Mo(VI) to Mo(IV). The S_2^{2-} species, as Schrader and Cheng (19) suggested from LRS characterization for the sulfided Mo/Al_2O_3 catalysts, exist on the surface oxygen vacancies and are related to the sulfidation extent of molybdenum oxide. The decrease in the S_2^{2-} amount with increasing potassium loading actually indirectly reflects the inhibition effect of the potassium promoter on the transformation of Mo(VI) to Mo(IV). As to the sulfidation of Mo(VI) to Mo(IV), an intermediate step of Mo(VI) to Mo(V) has been tentatively proposed by Massoth and co-workers (25). The K–Mo interaction is not favorable to the complete transformation of Mo(V) to Mo(IV) and results in the increase in Mo(V) ESR intensities of the potassium-promoted sulfided samples. At a K/Mo ratio above 0.8, the continuous resistance to sulfidation as indicated by the decrease in S^{2-}/Mo and S_2^{2-}/Mo ratios and increase in Mo(V) ESR intensity suggests that the formed KCl which does not completely aggregate into crystallites may partly cover the exposed molybdenum surface and inhibit the exchange of sulfur and oxygen atoms during sulfidation.

3. Effect of K–Mo Interaction on the Aggregation of Molybdenum Species

The XRD and LRS results clearly demonstate that the potassium promoter in the oxidic samples promotes aggregation of the molybdenum species to form the K–Mo interaction species. Compared to the sulfidation of the molybdenum species on the unpromoted sample, the sulfidation of the K–Mo interaction species gives rise to the aggregation of MoS_2 crystallites, as indicated by LRS measurements. As many studies revealed, the so-called coordinately unsaturated molybdenum (Mo(CUS)) sites are formed on the MoS_2 surface during sulfidation, where the chemisorption of the probe molecules could occur (34, 35). The uptakes of O_2 and CO at a low temperature of −83.6°C are related to the amount of Mo(CUS) sites on the sulfided samples (34, 36). From the fact that adding potassium promoter to the samples results in the decreases in the uptakes of both O_2 and CO on the sulfided samples, as shown in Fig. 8, it can be deduced that the potassium promoter promotes the aggregation of molybdenum disulfide and makes the number of the Mo(CUS) sites decreased. At the high potassium loading corresponding to the saturation of the K–Mo interaction, the further decreases in the uptakes of O_2 and CO could be due to the coverage of the unaggregated KCl on part of the Mo(CUS) sites to which the O_2 and CO molecules do not have access. But with increasing potassium loading the decrease in the uptakes of both O_2 and CO at a K/Mo ratio above 0.65–0.8 is less rapid than at lower potassium loadings (Fig. 8). This suggests that the effect of KCl coverage on Mo(CUS) sites is less significant than that of molybdenum aggregation. At a high temperature of 300°C, the adsorbed H_2 possibly dissociates on the Mo (CUS) sites and then, by spillover or other ways, migrates to the basal plane, where it bonds with sulfur atoms and remains as SH groups (37, 38). A multilayer growth of MoS_2 crystallites perpendicular to the basal plane is unfavorable to H_2 adsorption. Thus the amount of H_2 adsorption is affected by two factors, the number of surface Mo(CUS) sites and the migration of adsorbed hydrogen from Mo(CUS) sites to the surface where sulfur atoms

stay. Obviously, the decrease in the uptake of H_2 upon adding the potassium promoter to the samples reflects the aggregation of molybdenum disulfide, but because of the difference in H_2 adsorption mechanism from both O_2 and CO, the H_2 uptake linearly decreases as potassium loading increases.

In view of the mechanism of H_2 adsorption on the molybdenum sulfided, the two desorption species revealed in H_2 TPD for the sulfided samples (Fig. 9) could be ascribed, as recognized by some authors (30, 39), to the desorption of the dissociated hydrogen on Mo(CUS) sites (300–500°C) and H_2S (>450°C) relating to the surface SH groups. The decrease in the amount of both desorption species gives a conclusion similar to that from H_2 uptake data that the potassium component promotes aggregation of the sulfided molybdenum species and that at high potassium loading the unaggregated KCl could cover a part of the Mo(CUS) sites.

4. *Effect of K–Mo Interaction on the Catalytic Properties for Alcohol Synthesis*

The alcohol yield achieved on the sulfided samples (Fig. 10) is to some extent proportional to the amount of the formed K–Mo interaction species on the oxidic samples, the maximum occurring at K/Mo ratio of 0.8 which corresponds to the saturation of the K–Mo interaction. The formed KCl at high potassium loadings, as discussed above, is unfavorable to the formation of K–Mo interaction species and even covers the exposed molybdenum surface and hence decreases the alcohol yield. The good correlation between the activity toward alcohol formation and the amount of the K–Mo interaction species clearly indicates that the sulfided K–Mo species resulting from the precursor of oxidic K–Mo interaction is responsible for producing alcohols. According to Klier *et al.* (5), an interaction occurs on the alkali/MoS_2 catalysts between MoS_2, which is responsible for the H_2 activation, and the alkali component, which is responsible for CO activation. The maximal alcohol yield was observed at the certain alkali loading at which the two components display an optimal synergistic interaction. Xie *et al.* (6) proposed an surface species resulting from an interaction among the Mo^{6+}, K^+, S_2^{2-}, and O^{2-} which is responsible for the alcohol activity. The active sites or species for alcohol synthesis is still disputable. On the basis of the XPS results in the present work, it is plausible to conclude that the potassium-enriched surface "K–Mo–S" species may be responsible for alcohol formation. The MoS_2 crystallite size could be regarded as an indication of the amount of the "K–Mo–S" species in view of the case of Co–Mo/Al_2O_3 catalysts on which the amount of the "Co–Mo–S" species, an active species for the hydrodesulphurization reaction, is to some extent in proportional to the size of the MoS_2 crystallites. The inverse change of the hydrocarbon and alcohol activities with potassium loading strongly suggests that the active sites or species for both product formations is not identical at all. The linear variation of methanation and hydrogenation activities over supported sulfided Mo/Al_2O_3 and unsupported MoS_2 catalysts versus O_2 uptake at low temperatures (30, 40) tentatively suggest that the surface Mo(CUS) sites are responsible for the hydrocarbon formation. The K–Mo interaction promotes aggregation of the molybdenum disulfide and results in the decrease of the Mo(CUS) sites and thus decreases the activity for hydrocarbon formation. At a K/Mo ratio above 0.8, the decreases in both hydrocarbon and alcohol activities could be attributed to the coverage of the KCl on part of the Mo(CUS) sites and the "K–Mo–S" species. The large increase in alcohol selectivity at a K/Mo ratio above 0.8, as shown in Fig. 10, allows us to conclude that the former effect is much more significant than the latter in this range of K/Mo ratio. The variation of the alcohol selectivity versus potassium loading is similar to that obtained over the reduced K–Mo/SiO_2 and that over the sulfided K–Mo/ZrO_2 catalysts (7, 8), but different from that over unsupported K_2CO_3/MoS_2, and K_2CO_3/Mo_2C catalysts (6, 9). In the latter cases the alcohol selectivity decreases substantially at high potassium loadings.

Rather differently from unsupported molybdenum sulfide catalysts, the sulfided samples described in the present work display a very good property for producing $C_{2+}OH$ alcohols, as shown in Fig. 10. Over the sulfided sample with a K/Mo ratio of 0.8, the CO hydrogenation at 4.0 MPa, 280°C, 4500 h^{-1} for 100 h gives rise to a $C_{2+}OH$ percent in the alcohol product distribution above 80% (8); in contrast, over the unsupported molybdenum sulfide catalysts such as Cs/MoS_2 and K_2CO_3/MoS_2 etc. (5, 6), the $C_{2+}OH$ products less than 50–60% are generally obtained, and the main product is methanol. Murchison *et al.* (41) found that the $C_{2+}OH$ yield can be enhanced by introducing H_2S into the reactant mixture. Jalowiechi *et al.* (42) studied the treatment of the molybdenum sulfide catalysts with H_2 and revealed that the supported MoS_2/Al_2O_3 catalysts can store a much larger amount of H_2 than the unsupported MoS_2 catalysts. The TPD results shown in Fig. 9 indicate that on the sulfide samples treated with H_2, there is substantial amount of SH species which can desorbed, while the TPD of the unsupported K_2CO_3/MoS_2 catalysts performed under similar conditions gives no desorption species, which could be due to the surface SH species. In light of the above, the high $C_{2+}OH/C_1OH$ ratios in the alcohol product distribution could be attributed to the presence of the substantial amount of SH species formed on the surface of the sulfided samples during reaction in CO/H_2. In fact, the increase of methanol yield with increasing potassium loading, as shown in Fig. 10, is probably due to the decrease in the amount of SH species existing on the sample, as indicated in Fig. 9.

CONCLUSIONS

An interaction between the potassium promoter and the molybdenum oxo component supported on γ-Al_2O_3 results in the formation of a K–Mo interacting species related to $Mo_7O_{24}^{6-}$ and becomes saturated at the KCl loading with a K/Mo atomic ratio of 0.8. During sulfidation, MoS_2 crystallites and "K–Mo–S" species are formed. At a K/Mo ratio above 0.8, potassium remains in the KCl forms. A part of the formed KCl aggregates into crystallites; the others exist randomly on the sample surface and cover the exposed molybdenum surface and retard the sulfidation and reduction of Mo(VI) to Mo(IV).

The "K–Mo–S" species, generated from the sulfidation of the K–Mo interaction species, is active for the formation of alcohols from CO hydrogenation, while the Mo(CUS) sites could be responsible for the formation of hydrocarbons. At high potassium loadings, the unaggregated KCl has preferential coverage on the Mo(CUS) sites and results in a large increase in the alcohol selectivity. The high $C_{2+}OH/C_1OH$ ratio in alcohol product distribution could be attributed to the substantial amount of SH groups present on the supported sulfided samples.

ACKNOWLEDGMENTS

Support from the National Natural Science Foundation of China is gratefully acknowledged. We also thank Professor Cun-yi Xu, Mingrong Ji, and Gui-en Zhou for obtaining LRS, XPS, and XRD spectra.

REFERENCES

1. Quarderer, G. J., and Cochran, K. A., Eur. Patent 119 609 (1984).
2. Stevens, R. R., Eur. Patent 172 431 (1986).
3. Kinkade, N. E., Eur. Patents 149 255 and 149 256 (1985).
4. Xie, Y., Naasz, B. M., and Somorjai, G. A., *Appl. Catal.* **27,** 233 (1986).
5. Klier, K., Herman, R. G., Nunan, J. G., Smith, K. J., Bogdan, C. E., Young, C. W., and Santiesteban, J. G., *in* "Methane Conversion" (D. M. Bibby, C. D. Chang, R. F. Howe, and S. Y. Yurchak, Eds.), p. 109. Elsevier, Amsterdam, 1988.
6. Duan, L., Zhang, O., Ma, S., Li, S., and Xie, Y., *J. Mol. Catal. (China)* **4,** 208 (1990).
7. Muramatsu, A., Tatsumi, T., and Tominaga, H., *Bull. Chem. Soc. Jpn.* **60,** 3157 (1987).
8. Bian, G. Z., Jiang, M., Fu, Y. L., Omata, K., and Fujimoto, K., *J. Fuel Chem. Technol. (China)*, in press.
9. Woo, H. C., Park, K. Y., Kim, Y. G., Nam, I. S., Chung, J. S., and Lee, J. S., *Appl. Catal.* **75,** 267 (1991).
10. Tatsumi, T., Muramatsu, A., and Tominaga, H., *Appl. Catal.* **34,** 77 (1987).
11. DeCanio, S. J., Cataloo, M. C., DeCanio, E. C., and Storm, D. A., *J. Catal;*. **119,** 256 (1989).
12. Kantschewa, M., Delannay, F., Jeziorowski, H., Delgado, E., Eder, S., Ertle, G., and Knozinger, H., *J. Catal.* **87,** 482 (1984).
13. Tatsumi, T,. Muramatsu, A., and Tominaga, H., *J. Catal.* **101,** 553 (1986).
14. Wagner, C. D., Riggs, W. M., Davis, L. E., Moulder, J. F., and Muilenberg, G. E., *in* "Handbook of X-ray Photoelectron Spectroscopy." Perkin–Elmer Corporation, Physical Electronics Division, U.S.A., 1979.
15. Cheng, C. P., and Schrader, G. L., *J. Catal.* **60,** 276 (1979).
16. Wang, L., and Hall, W. K., *J. Catal.* **66,** 251 (1980).
17. Brown, F. R., Makovsky, L. E., and Rhee, K. H., *J. Catal.* **50,** 162 (1977).
18. Fu, Y. L., and Zhao, F. G., *Catal. Lett.* **12,** 117 (1992).
19. Schrader, G. L., and Cheng, C. P., *J. Catal.* **80,** 369 (1983).
20. Kim, D. S., Segawa, K., Soeya, T., and Wachs, I. E., *J. Catal.* **136,** 539 (1992).
21. Spevack, D. S., and McIyre, S., *Appl. Catal.* **64,** 191 (1990).
22. Muller, A., and Diemann, E., *in* "Advances in Inorganic Chemistry" (H. J. Emeleus and A. G. Sharpe, Eds), Vol. 31, p. 89. Academic Press, New York, 1987.
23. Okamoto, Y., Tomioka, H., Katoh, Y., Imanaka, T., and Teranishi, S., *J. Phys. Chem.* **84,** 1833 (1980).
24. Spevack, P. A., and McIntyre, S., *Appl. Catal.* **64,** 191 (1990).
25. Seshadri, K. S., Massoth, F. E., and Petrakis, L., *J. Catal.* **19,** 95 (1970).
26. Ismail, H. M., Zaki, M. I., Bond, G. C., and Shukri, R., *Appl. Catal.* **72,** L1 (1991).
27. Zmierzcak, W., Muralidhar, G., and Massoth, F. E., *J. Catal.* **77,** 423 (1982).
28. Bodrero, T. A., and Bartholomew, C. H., *J. Catal.* **84,** 145 (1983).
29. Reddy, B. M., Chary, K. V. R., Subrahmanyam, V. S., and Nag, N. K., *J. Chem. Soc. Faraday Trans. I* **81,** 1655 (1985).
30. Fu, Y. L., Tang, X. B., Huang, Z. G., and Fan, C. Z., *Appl. Catal.* **55,** 11 (1989).
31. Tatsumi, T., Muramatsu, A., Kokota, K., and Tominaga, H., *in* "Methane Conversion" (D. M. Bibby, C. D. Chang, R. F. Howe, and S. Y. Yurchak, Eds.), p. 219. Elsevier, Amsterdam, 1988.
32. Xie, X., Yin, H., and Huo, J., *J. Fuel Chem. Technol. (China)* **19,** 304 (1991).
33. Caceres, C. V., Fierro, L. G., Lazaro, J., Agudo, A. L., and Soria, J., *J. Catal.* **122,** 113 (1990).
34. Ratnasamy, P., and Sivassanker, S., *Catal. Rev.-Sci. Eng.* **22,** 401 (1980).
35. Valyon, J., and Hall, W. K., *J. Catal.* **84,** 216 (1983).
36. Zaki, M. I., Vielhaber, B., and Knözinger, H., *J. Phys. Chem.* **90,** 3176 (1986).
37. Wright, C. J., Sampson, C., Fraser, D., Moyes, R., Wells, P. B., and Richel, C., *J. Chem. Soc. Faraday Trans. I* **76,** 1585 (1980).
38. Wright, C. J., Fraser, D., Moyes, R., and Wells, P. B., *Appl. Catal.* **1,** 49 (1981).
39. Yerofeyev, V. I., and Kaletchits, I. V., *J. Catal.* **86,** 55 (1984).
40. Concha, B. E., Bartholomew, G. L., and Bartholomew, C. H., *J. Catal.* **89,** 536 (1984).
41. Murchison, C. B., Conway, M. M., Stevens, R. R., and Quarderer, G. J., *in* "Proceedings, 9th International Congress on Catalysis, Calgary, 1988" (M. J. Phillips and M. Ternan, Eds.), Vol. 2, p. 626. Chem. Institute of Canada, Ottawa, 1988.
42. Jalowiecki, L., Grimblot, J., and Bonnelle, S. P., *J. Catal.* **126,** 101 (1990).